

## RESEARCH ARTICLE

10.1002/2017JA024754

## Key Points:

- Case studies of relativistic microbursts with EMIC and/or chorus waves occurring are presented
- Statistically, there is an increase in VLF wave amplitude at the time of relativistic microbursts, consistent with chorus
- Statistically, there is no increase in EMIC activity at the time of relativistic microbursts

## Correspondence to:

E. Douma,  
emmadouma@gmail.com

## Citation:

Douma, E., Rodger, C. J., Clilverd, M. A., Hendry, A. T., Engebretson, M. J., & Lessard, M. R. (2018). Comparison of relativistic microburst activity seen by SAMPEX with ground-based wave measurements at Halley, Antarctica. *Journal of Geophysical Research: Space Physics*, 123, 1279–1294. <https://doi.org/10.1002/2017JA024754>

Received 6 SEP 2017

Accepted 31 JAN 2018

Accepted article online 5 FEB 2018

Published online 22 FEB 2018

## Comparison of Relativistic Microburst Activity Seen by SAMPEX With Ground-Based Wave Measurements at Halley, Antarctica

Emma Douma<sup>1</sup> , Craig J. Rodger<sup>1</sup> , Mark A. Clilverd<sup>2</sup> , Aaron T. Hendry<sup>1</sup> , Mark J. Engebretson<sup>3</sup> , and Marc R. Lessard<sup>4</sup>

<sup>1</sup>Department of Physics, University of Otago, Dunedin, New Zealand, <sup>2</sup>British Antarctic Survey, NERC, Cambridge, UK, <sup>3</sup>Department of Physics, Augsburg University, Minneapolis, MN, USA, <sup>4</sup>Department of Physics, University of New Hampshire, Durham, NH, USA

**Abstract** Relativistic electron microbursts are a known radiation belt particle precipitation phenomenon; however, experimental evidence of their drivers in space have just begun to be observed. Recent modeling efforts have shown that two different wave modes (whistler mode chorus waves and electromagnetic ion cyclotron (EMIC) waves) are capable of causing relativistic microbursts. We use the very low frequency/extremely low frequency Logger Experiment and search coil magnetometer at Halley, Antarctica, to investigate the ground-based wave activity at the time of the relativistic microbursts observed by the Solar Anomalous Magnetospheric Particle Explorer. We present three case studies of relativistic microburst events, which have one or both of the wave modes present in ground-based observations at Halley. To extend and solidify our case study results, we conduct superposed epoch analyses of the wave activity present at the time of the relativistic microburst events. Increased very low frequency wave amplitude is present at the time of the relativistic microburst events, identified as whistler mode chorus wave activity. However, there is also an increase in Pc1–Pc2 wave power at the time of the relativistic microburst events, but it is identified as broadband noise and not structured EMIC emissions. We conclude that whistler mode chorus waves are, most likely, the primary drivers of relativistic microbursts. However, case studies confirm the potential of EMIC waves as an occasional driver of relativistic microbursts.

### 1. Introduction

Relativistic electron microbursts are small-timescale ( $< 1$  s) intense precipitation events of  $> 1$  MeV electrons from the outer radiation belt into the atmosphere (Blake et al., 1996), typically observed in morning magnetic local times (MLT) (Blum et al., 2015; Johnston & Anderson, 2010; Nakamura et al., 2000; O'Brien et al., 2003; Thorne et al., 2005). It is believed relativistic electron microbursts are significant contributors to radiation belt losses, with the suggestion that a single storm containing relativistic microbursts could empty the entire outer radiation belt relativistic electron population (Clilverd et al., 2006; Dietrich et al., 2010; Lorentzen, Looper, & Blake, 2001). The net flux in the radiation belts is delicate balance between loss and energization (Reeves et al., 2003); therefore, we require better understanding of the conditions under which relativistic microbursts occur, and moreover, the physical processes in space driving this type of precipitation.

It is well known that lower-energy electron microbursts (energy of tens to hundreds of keV) are a result of wave particle interactions with whistler mode chorus waves (Fennell et al., 2014; Lorentzen, Blake, et al., 2001). For some time it has been suggested that relativistic microbursts are also a result of pitch angle scattering of radiation belt electrons by whistler mode chorus waves. However, there is little direct experimental evidence in the existing literature to demonstrate this. There are a number of experimental studies published in support of the chorus wave driver of relativistic microbursts. These are primarily based on the overlap in  $L$  and MLT of large-scale regions of relativistic microburst occurrence and whistler mode chorus wave occurrence or power (e.g., Anderson et al., 1977; Johnston & Anderson, 2010; Kersten et al., 2011; Kurita et al., 2016; Lorentzen, Blake, et al., 2001; Nakamura et al., 2000). A recent study by Breneman et al. (2017) shows the first direct evidence of simultaneous observations of relativistic microbursts and whistler mode chorus waves during a single case study. Modeling efforts show that rising tone elements of whistler mode chorus waves propagating away from

the equator along the field line (high magnetic latitude) can cause relativistic microbursts at the same time as low-energy microbursts (Kersten et al., 2011; Lorentzen, Blake, et al., 2001; Miyoshi et al., 2015; Nakamura et al., 2000; Saito et al., 2012; Thorne et al., 2005). Although, there is an absence of simultaneous  $< 100$  keV precipitating electrons in subionospheric observations during two relativistic microburst precipitation events studied in detail by Rodger et al. (2007), recent observations by Focused Investigations of Relativistic Electron Bursts: Intensity, Range, and Dynamics II have shown microburst precipitation spanning 200 keV to 1 MeV (Crew et al., 2016).

Recently, Omura and Zhao (2013) focused upon anomalous cyclotron resonance between relativistic electrons ( $> 1$  MeV) and electromagnetic ion cyclotron (EMIC)-triggered emissions. These authors reported that this resonance is highly effective and should result in the efficient precipitation of relativistic electrons through nonlinear trapping by coherent EMIC-triggered emissions as they increase in frequency. This work has been expanded upon in Kubota and Omura (2017), who found that a combination of nonlinear EMIC wave trapping and scattering at low pitch angles can cause relativistic microbursts. Douma et al. (2017) have undertaken an in-depth study of relativistic microburst occurrence distribution over  $L$  and MLT and compared this to the EMIC wave (and chorus wave) distributions. They have shown that microbursts occurring in the 8–17 MLT region are consistent with scattering by EMIC waves, while microbursts occurring in the 8–13 MLT or 22–24 MLT region are consistent with scattering by either whistler mode chorus or EMIC waves. These comparatively new studies indicate that there is uncertainty as to the dominant scattering process which leads to relativistic microbursts, suggesting that the occurrence of these precipitation events should be further examined.

For reference, whistler mode chorus waves are electromagnetic emissions characterized by a sequence of discrete elements typically in the range  $0.1$ – $0.8 f_{ce}$  (where  $f_{ce}$  is the electron gyrofrequency) (Santolik et al., 2003). They are observed in two different bands: above (upper band) and below (lower band) half the electron gyrofrequency (Tsurutani & Smith, 1974). The generation region of chorus is located outside the plasmopause near the geomagnetic equator (LeDocq et al., 1998; Santolik et al., 2003) and is associated with enhanced fluxes of suprathermal electrons injected from the plasma sheet (Anderson & Maeda, 1977). Chorus waves have been observed to occur mainly on the morningside MLT (0000–1200 MLT) and across a wide range of  $L$  shells (Li et al., 2009). EMIC waves are Pc1–Pc2 (0.1–5 Hz) waves that are generated near the magnetic equator by anisotropic ring current protons (Jordanova et al., 2008). The waves are generated in three different frequency bands: below the hydrogen, helium, and oxygen ion gyrofrequencies, respectively. EMIC waves have been observed across a wide range of  $L$  shells (Meredith et al., 2014; Usanova et al., 2012), and recent studies have shown that the occurrence of EMIC events is higher on the dayside than the nightside of the magnetosphere (Saikin et al., 2015).

In our study we address this lack of direct comparison between relativistic electron microbursts and potential wave drivers. Due to the difficulty of comparing measurements from moving satellite platforms, we choose to use a Low Earth Orbiting satellite and ground-based observations for our comparison. We will begin by presenting three case study events with differing radio wave conditions. We will present an example of whistler mode chorus waves at a similar time to the microburst activity, an example of EMIC waves at a similar time to the microburst activity, and an example of both EMIC and chorus waves at a similar time to the microburst activity. Based on these case studies it is unclear which plasma wave is the primary driver of the relativistic microbursts. Thus, we will expand our investigation from the three case studies to a large statistical analysis of the whistler mode chorus and EMIC wave activity present at Halley, Antarctica, during the time of the observed relativistic microbursts. In particular, we will focus on superposed epoch analyses of the wave activity present at the time of observed relativistic microbursts that occurred close to Halley or its magnetic conjugate.

## 2. Instrumentation

In this study, we follow the method outlined in Douma et al. (2017) to identify relativistic microbursts. We use the  $> 1$  MeV electron flux channel on the Solar Anomalous Magnetospheric Particle Explorer (SAMPEX) satellite. A detailed instrument description of the Heavy Ion Large Telescope instrument and SAMPEX spacecraft is given in Klecker et al. (1993) and Baker et al. (1993) and summarized in Douma et al. (2017) along with a detailed description of the detection algorithm used. The algorithm employed is an application of the work undertaken by O'Brien et al. (2003) and Blum et al. (2015). The O'Brien et al. (2003) algorithm given in equation (1), where  $N_{100}$  is the number of counts in 100 ms and  $A_{500}$  is the centered running average of  $N_{100}$  over five 100 ms intervals, is applied to all the SAMPEX Heavy Ion Large Telescope data from 23 August 1996

to 11 August 2007. Note, however, that the detection algorithm does not perform well at either low radiation belt fluxes or during strong pitch angle diffusion (O'Brien et al., 2003).

$$\frac{N_{100} - A_{500}}{\sqrt{1 + A_{500}}} > 10 \quad (1)$$

In the current study we no longer make use of the 193,694 individual microbursts but combine the relativistic microbursts into sets of microbursts we term “events” to avoid double counting in any accompanying wave analysis (i.e., to ensure the same wave event is not included in the data set more than once). An event is defined as a group of microbursts occurring within a 4 min window (roughly equivalent to one pass of SAMPEX through the outer radiation belt). We have a total of 22,023 relativistic microburst events observed between the start of 1996 and the end of 2007, which is a combination of 193,694 individual microbursts. From the start of 2005 to the end of 2007 we only have 4,199 relativistic microburst events, a combination of 32,871 individual microbursts.

The wave analysis is achieved using the scientific instruments at the British Antarctic Base, Halley, located at a geographic location of  $-75.5^{\circ}\text{N}$  and  $333.4^{\circ}\text{E}$ . It is situated at an  $L$  of 4.56 and an MLT of 1444 at local noon universal time (UT) (Engebretson et al., 2008). In particular, we use two ground-based wave detection instruments: the very low frequency/extremely low frequency (VLF/ELF) Logger Experiment (VELOX) and the search coil magnetometer (SCM).

Both whistler mode chorus and EMIC waves propagate from their respective generation regions into both hemispheres (Loto'aniu et al., 2005). Therefore, we must also investigate relativistic microbursts occurring at Halley's magnetic conjugate location in the Northern Hemisphere. We use the International Geomagnetic Reference Field (IGRF) model ([https://omniweb.gsfc.nasa.gov/vitmo/cgm\\_vitmo.html](https://omniweb.gsfc.nasa.gov/vitmo/cgm_vitmo.html)) at SAMPEX altitude for each year in our analysis to determine that Halley's magnetic conjugate location is at average geographic coordinates of  $55.2^{\circ}\text{N}$  and  $304.4^{\circ}\text{E}$ .

The Halley SCM started operation in February 2005 and continued to take measurements through until January 2017. It is capable of measuring wave power in the Pc1–Pc2 frequency range (EMIC waves). There were some significant outages in measurements during this time window and periods of unusable data due to calibration or other issues. The main period of unusable data affecting our 2005–2007 analysis is from April 2005 to June 2005, with only a few days of good data existing over these months. This data outage was due to an electrical grounding problem which caused the amplitude to decrease drastically (Engebretson et al., 2008). By rescaling the color bar of the quick look plots, we can restore readability of the images, however, as the exact scaling is unknown we were unable to use these days in our superposed epoch analyses (section 4.2).

The Halley VELOX started operation in 1992 and continued to take measurements through until 2007, when it was replaced with the VELOXnet instrument. A detailed instrument description of VELOX is given in Smith (1995) and summarized here. VELOX has eight logarithmically spaced frequency bands (0.5, 1, 1.5, 2, 3, 4.25, 6, and 9.3 kHz) with an amplitude resolution of 0.376 dB, where the 0 dB reference level is  $10^{-33} \text{ T}^2 \text{ Hz}^{-1}$ . The system noise level is 15–20 dB, and the saturation level is  $\sim 75$  dB. VELOX measures the average log amplitude occurring in each frequency channel at 1 s resolution. The upper frequency channels (6 kHz and 9.3 kHz) are dominated by thunderstorm noise (spherics) which are strongest at night and largely repeatable from day to day. The lowest frequency channel (0.5 kHz) is affected by spherics and ELF hiss (and occasionally by wind noise), and the measured amplitude remains relatively constant over time. In the middle frequency channels (1–4 kHz) the influence of distant spheric noise is reduced by attenuation in the Earth-ionosphere waveguide. Thus, these channels are dominated by magnetospheric emissions, namely, whistler mode hiss and chorus (Smith et al., 2004). Note, however, that the 1 s temporal resolution of VELOX is not sufficient to distinguish between the two; that is, VELOX cannot detect the high time resolution variation of the chorus elements.

### 3. Case Studies

Previous studies presented in the literature have found relativistic microbursts occurring coincident in time with whistler mode chorus waves. In particular, Lorentzen, Blake, et al., (2001) presented case studies of relativistic microburst observations made by SAMPEX and whistler mode chorus waves observed on Polar occurring in a similar local time sector, separated by 1–3  $L$  and 1 MLT. Kersten et al. (2011) showed case studies of relativistic microburst observations made by SAMPEX at similar  $L$  shell but separated by 1–5 MLT

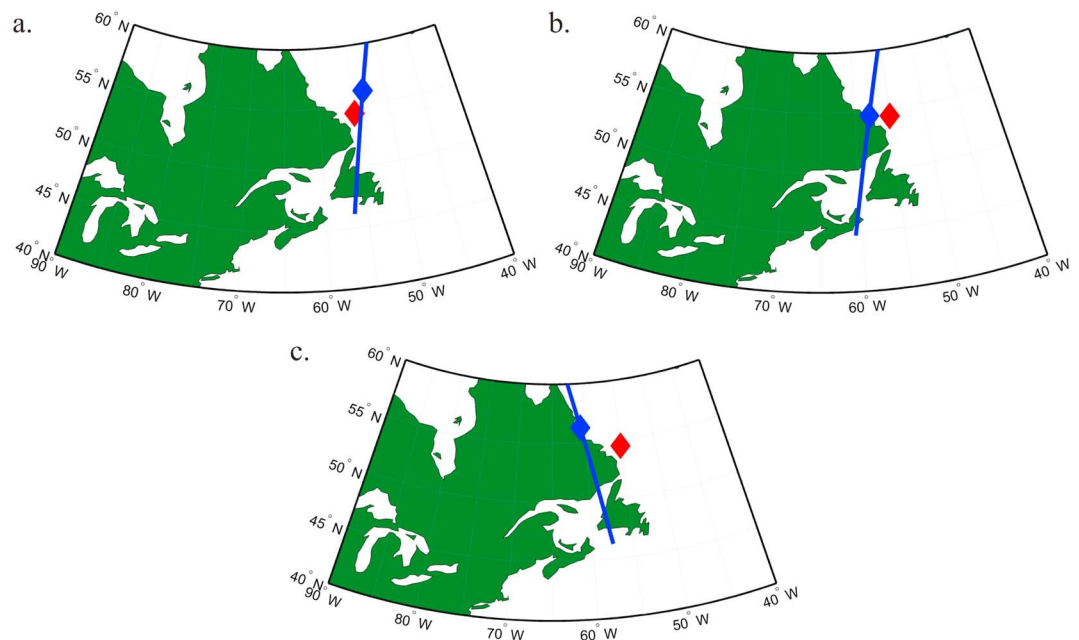


**Figure 1.** Maps of the SAMPEX satellite track (blue line), the location of the SAMPEX observed microburst (blue diamond), and Halley's conjugate location (red diamond, off the east coast of Canada) for the case study events on (a) 2 March 2005, (b) 1 July 2005, and (c) 19 May 2005.

with whistler mode chorus waves observed by the Solar Terrestrial Relations Observatory. Here we present one such case study of relativistic microbursts observed by SAMPEX occurring concurrently with whistler mode chorus wave observations made on the ground at Halley. In addition, we present case studies of relativistic microbursts observed by SAMPEX and concurrent EMIC wave observations on the ground, which, to the best of the authors knowledge, are missing in the existing literature. The EMIC wave activity has been investigated within a 2 h window of the relativistic microburst event to allow comparison of the results with Hendry et al. (2016). For consistency we have also investigated the chorus wave activity within a 2 h window of the relativistic microburst event. In the following three case studies the detected microbursts have essentially the same time duration and structure despite the apparent differences in the scattering mechanisms.

It will be important to note whether the relativistic microbursts in the case studies are occurring during the day ionosphere or night ionosphere. The absorption of VLF and ULF (in the Pc1 – Pc2 frequency range) signals is higher during the day for penetration through the ionosphere when compared to the night ionosphere (Engebretson et al., 2008; Smith et al., 2010). Thus, in the day ionosphere we will have reduced penetration of the VLF/ULF waves through the *D* region ionosphere which will result in reduced detection of VLF/ULF waves on the ground. We calculate the solar zenith angle at 100 km for each case study to describe the state of ionospheric conditions. Solar zenith angle  $<90^\circ$  indicates a sunlit ionosphere, solar zenith angle  $>108^\circ$  indicates a dark ionosphere, and angles between these indicates that the ionosphere is transitioning from sunlight to darkness (following Seppälä et al., 2008). All three of our case studies occur during low *Dst* and *Kp* activity, and elevated *AE* activity.

### 3.1. Case 1: Whistler Mode Chorus Wave Activity Only

The first case study we present occurred on 2 March 2005 at 12:25:56 UT, during sunlight conditions at Halley (solar zenith angle of  $60.6^\circ$  at 100 km). At the start of the microburst event SAMPEX was located at a latitude of  $56.1^\circ\text{N}$  and a longitude of  $306.6^\circ\text{E}$ , as shown in Figure 1a. At the altitude of SAMPEX there is  $1.8^\circ$  latitude and  $1.6^\circ$  longitude separation between the SAMPEX location (at the start of the microburst event (blue diamond)) and Halley's magnetic conjugate location (red diamond). SAMPEX observed the relativistic microburst event while at an average IGRF *L* of 5.8 (the event was seen from  $L = 5.3$ – $6.3$ ). Figure 2a presents the  $> 1$  MeV flux observed by SAMPEX during the time of this microburst event, with the microburst algorithm triggers (described in more detail in Douma et al., 2017) indicated by the red crosses. This microburst event consists of 16 individual microbursts detected by the algorithm, occurring during an *AE* index value of 298 nT

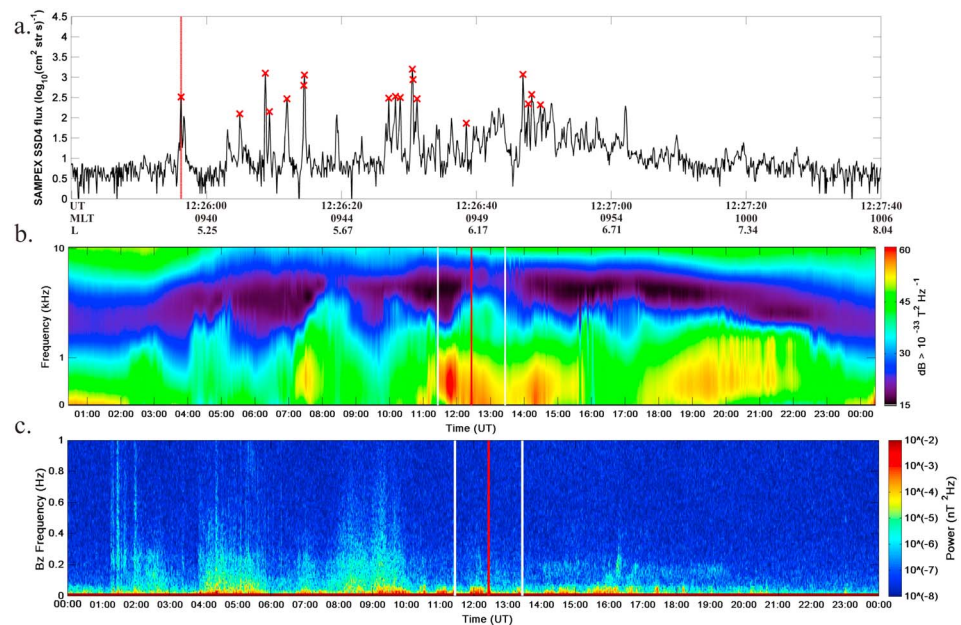


**Figure 2.** (a) The SAMPEX > 1.05 MeV electron flux (log scale) on 2 March 2005, with each red cross indicating a microburst reported by the algorithm. The red line identifies the onset of the relativistic microburst event. (b) Halley VELOX quick look plot of the wave amplitude in the 1–10 kHz frequency range on 2 March 2005. The red line identifies the start of the relativistic microburst event, and the two white lines indicate  $\pm 1$  h from event onset. (c) The spectrogram of the Bz component of the Halley magnetometer wave power in the 0–1 Hz frequency range on 2 March 2005. The red line identifies the onset of the relativistic microburst event and the two white lines indicate  $\pm 1$  h from event onset.

(*Dst* of  $-11$  nT, and *Kp* of 3). Although geomagnetic activity is low with the exception of *AE*, our case study occurs during sunlit conditions at Halley, and hence, we expect to see reduced penetration of the VLF/ULF waves as stated above.

Figure 2b presents the Halley VELOX quick look plot on 2 March 2005. The start of the relativistic microburst event (shown in Figure 2a) is identified by the red line in Figure 2b. Two white lines representing times 1 h prior and after the microburst event onset are shown. In Figure 2b we note a clear increase in the wave amplitude (above the background) in the 1–4 kHz frequency range during the 2 h window surrounding the relativistic microburst event. As noted previously, this increase in ground detected wave amplitude in the 1–4 kHz frequency range is an indication of either whistler mode chorus or hiss activity. We can further identify the wave activity by the delayed enhancement of wave power at higher frequencies in the 2–4 kHz frequency range inside this temporal window compared with the initial enhancement at  $\sim 0.5$  kHz. This rounded shape is identified as evidence of whistler mode chorus wave activity (see, e.g., Abel et al., 2006; Collier & Hughes, 2004; Smith et al., 1999). Although the ionosphere above Halley is sunlit during the relativistic microburst event, we have evidence of strong chorus wave activity detected on the ground.

We investigate the EMIC activity within a 2 h window of the relativistic microburst event onset following the analysis of Hendry et al. (2016), and to remain consistent with the chorus wave investigation. Figure 2c presents the Bz component of the Halley SCM spectrogram on 2 March 2005, where the relativistic microburst event is identified in the same way as Figure 2b. All three components of the magnetometer show the same wave power structure, but we have only presented the Bz component as it has the lowest noise. From Figure 2c it is clear there is no wave power present (above the background) inside the 2 h window of the relativistic microburst event start. As Halley is sunlit during this relativistic microburst event, the EMIC waves may not be able to penetrate the ionosphere and reach the ground (Engebretson et al., 2008). This could be the cause of our lack of EMIC wave observations in the Halley magnetometer.

Thus, we conclude that this satellite-observed relativistic microburst event was coincident with ground-based-detected whistler mode chorus waves, while no ground-based detected EMIC waves occurred in the same time period.

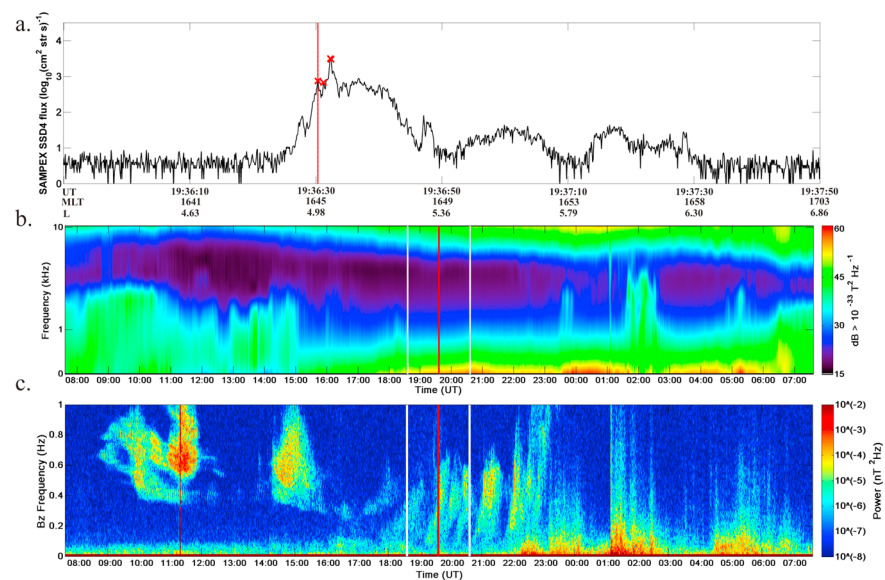


**Figure 3.** As Figure 2 but for the relativistic microburst event on 1 July 2005. Note in (b) and (c) the temporal range is from 08:00 UT, 1 July 2005 to 08:00 UT, 2 July 2005.

### 3.2. Case 2: EMIC Wave Activity Only

The second case study we present occurred on 1 July 2005 at 19:36:30 UT, during night conditions at Halley (solar zenith angle of  $109.5^\circ$  at 100 km). As the ionosphere is in darkness we will not discuss further the effects of transionospheric absorption. Figure 1b (similar to Figure 1a) shows at the start of the microburst event SAMPEX was located at a latitude of  $54.6^\circ\text{N}$  and a longitude of  $302.1^\circ\text{E}$ , with  $0.2^\circ$  latitude and  $2.9^\circ$  longitude separation between the SAMPEX location (at the start of the microburst event) and Halley's magnetic conjugate location (at SAMPEX altitude). SAMPEX observed the relativistic microburst event at an IGRF  $L$  of 4.99. The microburst event consisted of three individual microbursts detected by the algorithm shown in Figure 3a in the same way as Figure 2a. The relativistic microburst event occurred during a period with an  $AE$  value of 402 nT ( $Dst$  of  $-2$  nT, and  $Kp$  of  $4+$ ).

Although there is an underlying precipitation structure in Figure 3a, the individual bursts of precipitation last  $<1$  s, which is consistent with the definition of relativistic microbursts. Additionally, the small number of microbursts detected in this event is not uncommon. In fact, 60% of our relativistic microburst events contain less than five individual microbursts. This could be the result of SAMPEX passing through the edge of the larger microburst precipitation region. Alternatively, it could be the result of SAMPEX passing through microburst precipitation regions of differing sizes.

Figure 3b presents the Halley VELOX quick look plot from 08:00 UT, 1 July 2005 to 08:00 UT, 2 July 2005, in the same way as Figure 2b. In Figure 3b we note that there is no wave amplitude increase evident above the background level in the 1–4 kHz frequency range during the 2 h window surrounding the relativistic microburst event. Recall the ionosphere was not sunlit, and there was low geomagnetic activity so we would expect VLF waves to be able to penetrate the D-region of the ionosphere close to Halley.

Figure 3c presents the  $B_z$  component of the Halley SCM spectrogram from 08:00 UT, 1 July 2005 to 08:00 UT, 2 July 2005, following the layout of Figure 2c. Again, the  $B_z$  component had the lowest noise. Inside the 2 h window of the relativistic microburst event, the spectrogram shows clear bursts of wave power present in the Pc1–Pc2 frequency range. The rising tone structure and clear lower limit of the wave power is identified as IPDP (Intervals of Pulsations of Diminishing Periods) EMIC waves (Troitskaya, 1961). Assuming the microburst event observed by SAMPEX is caused by the EMIC wave, we can use the satellite location to estimate the ion gyrofrequencies at the IGRF-determined geomagnetic equator. The IGRF magnetic field at the geomagnetic equator was calculated using the International Radiation Belt Environment Modeling library (Boscher et al., 2015). Comparing the calculated ion gyrofrequencies with the frequency range of the EMIC wave observed at Halley, we find the EMIC wave is between the helium and oxygen ion gyrofrequencies, that is, is a Helium

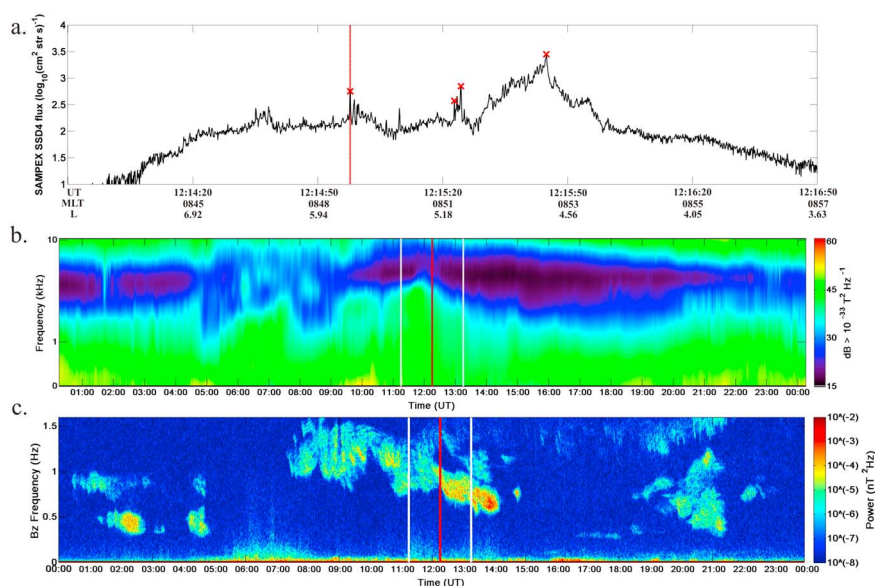


**Figure 4.** As Figure 2 but for the relativistic microburst event on 19 May 2005.

band EMIC wave. The EMIC wave was also found to be Helium band when the Tsyganenko 1989 magnetic field model was used (Tsyganenko, 1989).

Thus, we conclude that this satellite-observed relativistic microburst event was observed occurring concurrently with Helium band IPDP EMIC waves detected on the ground, while no concurrent whistler mode chorus waves were detected on the ground in the same time period. The authors believe this is the first published example of a relativistic microburst event which might be driven by an EMIC electron scattering mechanism proposed by Omura and Zhao (2013).

### 3.3. Case 3: Whistler Mode Chorus and EMIC Wave Activity

The third case study we present occurred on 19 May 2005 at 12:14:58 UT, during the recovery period of a geomagnetic storm (onset 15 May 2005, minimum  $Dst$   $-247$  nT). At this time, Halley was experiencing partial sunlight conditions (solar zenith angle of  $86.9^\circ$  at 100 km). Figure 1c (similar to Figure 1a) show the  $1.9^\circ$  latitude and  $5.7^\circ$  longitude separation between the SAMPEX location (at the start of the microburst event) and Halley's magnetic conjugate location (at SAMPEX altitude). SAMPEX observed the start of the relativistic microburst event at an IGRF  $L$  of 5.7, at a latitude of  $56.3^\circ$ N, and at a longitude of  $299.3^\circ$ E. The microburst event consisted of four individual microbursts detected by the algorithm, shown in Figure 4a (similar to Figure 2a). The relativistic microburst event occurred during a period with an  $AE$  index value of 188 nT ( $Dst$  of  $-37$  nT, and  $Kp$  of 2-).

Figure 4b presents the Halley VELOX quick look plot on 19 May 2005, following the layout of Figure 2b. In Figure 4b we note a slight increase in the wave amplitude (above the background) in the 1–4 kHz frequency range inside the 2 h window surrounding the relativistic microburst event. As in Case 1, the rounded shape of the wave amplitude in the 2–4 kHz frequency range inside this temporal window identifies it as whistler mode chorus wave activity.

Figure 4c presents the Bz component of the Halley SCM spectrogram on 19 May 2005, following the layout of Figure 2c. As the relativistic microburst event occurred during the recovery stage of a geomagnetic storm there is likely to be improved propagation of EMIC waves to the ground (Engebretson et al., 2008). In Figure 4c we can see bursts of Pc1–Pc2 wave power inside the temporal window of the microburst event. The clear lower limit of the wave power identifies it as an EMIC wave (Hendry et al., 2016), although not IPDP as in Case 2. If we assume the relativistic microburst event observed by SAMPEX is caused by the EMIC wave, we can use the satellite location to estimate the ion gyrofrequencies as before. Here we find that the EMIC wave is between the hydrogen and helium ion gyrofrequencies, that is, is a hydrogen band EMIC wave, for both the IGRF and Tsyganenko 1989 magnetic field models.

## 4. Statistical Data Processing

From the three presented case studies it is not clear whether the relativistic microburst events are primarily associated with whistler mode chorus waves, or EMIC waves, or equally associated with both chorus and EMIC waves. To investigate the chorus wave driver, we have expanded our analysis to cover the years from 1996 to 2007 where we have overlapping data from SAMPEX, and Halley VELOX. To investigate the EMIC wave driver, we reduce the temporal period to between 2005 and 2007, where we have a data overlap between SAMPEX and the Halley SCM.

### 4.1. Whistler Mode Chorus Wave Activity

In order to test the relationship between whistler mode chorus waves and relativistic microbursts, we undertake a superposed epoch analysis of the 1 min averaged wave amplitude in the 2 kHz channel of the Halley VELOX. We initially outline the algorithm used and any data processing and then discuss the results from the superposed epoch analysis. Recall that we cannot confirm the occurrence of whistler mode chorus waves through a superposed epoch analysis due to limitations of the VELOX instrument resolution. However, we can investigate the link between relativistic microbursts and VELOX reported VLF wave amplitude observed on the ground.

#### 4.1.1. Microburst Chorus Algorithm

The first step in our analysis is to limit our database of relativistic microburst events to those which occur close to Halley (or Halley's conjugate location). We map Halley's location (and Halley's conjugate location) to SAMPEX altitudes using a field line tracer based on the IGRF model using the year of the microburst event. We then define a relativistic microburst event as being close to Halley (and Halley's conjugate location) if it occurs within  $\pm 15^\circ$  longitude of Halley (or Halley's conjugate region). Note that  $\pm 15^\circ$  longitude is equivalent to  $\pm 1$  h in MLT (Hendry et al., 2016). This reduces our data set of relativistic microburst events to 2,239 events ( $\sim 10\%$  of the entire microburst database), resulting from a combination of 21,708 individual microbursts. We further limit our relativistic microburst database to events which occur in the  $L$  shell range of  $L = 4-5$  (i.e., close to the  $L$  of Halley), as whistler mode chorus waves propagate along a field-aligned path to lower altitudes (i.e., undergoes ducted propagation) (Smith et al., 2010). This reduces our data set of relativistic microburst events to 1,074 events (a combination of 9,228 individual microbursts).

Whistler mode chorus waves undergo strong attenuation as they propagate in the Earth-ionosphere waveguide to Halley (Smith et al., 2010). Figure 2b of Smith et al. (2010) indicates that the attenuation of the signals reaches a peak at 2 kHz. High attenuation limits the ability of the VLF waves to propagate horizontally in the Earth-ionosphere waveguide; thus, any signals received by VELOX in this frequency range should be entering the waveguide close to Halley. Furthermore, recall that the absorption of VLF signals is higher during day for penetration through the ionosphere when compared to the night ionosphere (Smith et al., 2010). This absorption difference will be of importance to our investigation as it will strongly influence the detection efficiency of the VELOX instrument. To address this issue, we have investigated the VLF wave amplitude in the 2 kHz frequency range at Halley separately for the Halley summer (November, December, January, and February) and winter (May, June, July, and August). Note that due to Halley's location the summer (winter) is largely sunlit (darkness). We have 242 relativistic microburst events during Halley winter and 170 relativistic microburst events during Halley summer.

We have also created a database of random epochs for both summer and winter. The random epochs have been constrained to the same season as the true microburst epochs. We have 242 random epochs during Halley winter and 170 random epochs during Halley summer. This will give us a baseline with which to compare the results of the superposed epoch analysis using the true microburst events.

The VELOX data have a resolution of 1 s with calibration tones occurring on each minute (1 s long), on each 10 min (3 s long), and on each hour (10 s long) (This information is supplied in the BAS data manual for VELOX, which is available on request.). To remove this calibration effect, we calculate the mean wave amplitude in the 2 kHz channel over each minute, removing the first 3 s of each minute and the first 10 s of each minute on the hour. Due to a slight drift in the VELOX clock over its lifetime, we must remove 3 s of data each minute to ensure the removal of both the 1 s and 3 s long calibration tones.

#### 4.1.2. Superposed Epoch Analysis

Presented here in Figure 5 is the superposed epoch analysis of the VLF wave amplitude in the 2 kHz channel of VELOX (Figures 5a and 5b) and its statistical significance (Figures 5c and 5d). The Halley winter (summer) relativistic microburst events are presented in Figures 5a and 5c (Figures 5b and 5d). The black line in Figures 5a

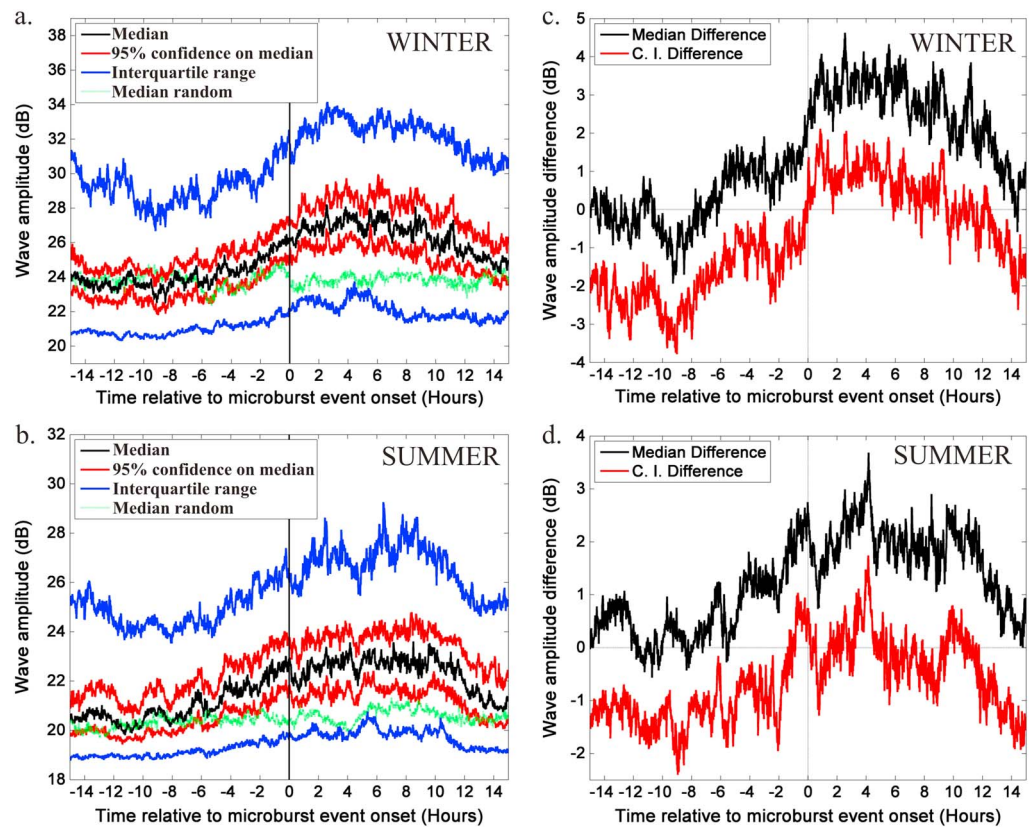


**Figure 5.** A superposed epoch study of the VLF wave amplitude in the 2 kHz channel of VELOX using the (a) winter time and (b) summer time relativistic microburst events. The median wave amplitude is given by the black line, the red lines are the 95% confidence interval on the median, the blue lines are the interquartile range, the green line is the median wave amplitude using the random epochs (baseline), and the black vertical line denotes the time of the relativistic microburst event onset, that is, the epoch. The black line in (c) winter and (d) summer is the median of the microburst events minus the median of the random events while the red line gives the lower 95% confidence interval (C.I.) of the microburst events minus the upper 95% C.I. of the random events.

and 5b is the median wave amplitude for  $\pm 15$  h from the time of the relativistic microburst event. The red lines indicate the 95% confidence interval on the median, and the blue lines indicate the interquartile range. The green line in Figures 5a and 5b is the median wave amplitude found using the random epochs (baseline). The black line in Figures 5c and 5d is the median wave amplitude of the microburst events minus the median wave amplitude of the random events. In contrast the red line shows the lower 95% confidence interval of the microburst events minus the upper 95% confidence interval of the random events. When the differences in the confidence intervals (red line in Figures 5c and 5d) are positive, the confidence intervals between the microburst events and the random events no longer overlap, and thus, the median wave amplitude difference is significant.

From Figure 5 it is clear that during both the Halley winter and Halley summer there is an increase in the 2 kHz median wave amplitude for relativistic microbursts events when compared to the random events. The increase in the 2 kHz median wave amplitude observed on the ground begins roughly 30 min (1 h) prior to the onset of winter (summer) relativistic microburst events seen during the satellite overpass. It remains elevated for  $\sim 9$  h ( $\sim 13$  h) following the winter (summer) microburst event epoch onset. The median wave amplitude reaches a peak  $\sim 4$  h after the onset for both summer and winter relativistic microburst events. However, there is a larger increase (average of 3.1 dB increase from the random events over the  $\sim 9$  h of elevation) in the median wave amplitude during the winter relativistic microburst events when compared to the summer relativistic microburst events (average of 2.0 dB increase from the random events over the  $\sim 13$  h of elevation). This difference is consistent with expected seasonal changes in ionospheric absorption. The difference between the median wave amplitudes for microburst events and random events is significant for  $\sim 9$  h following the start of the winter relativistic microburst events. For the summer events there are occasional

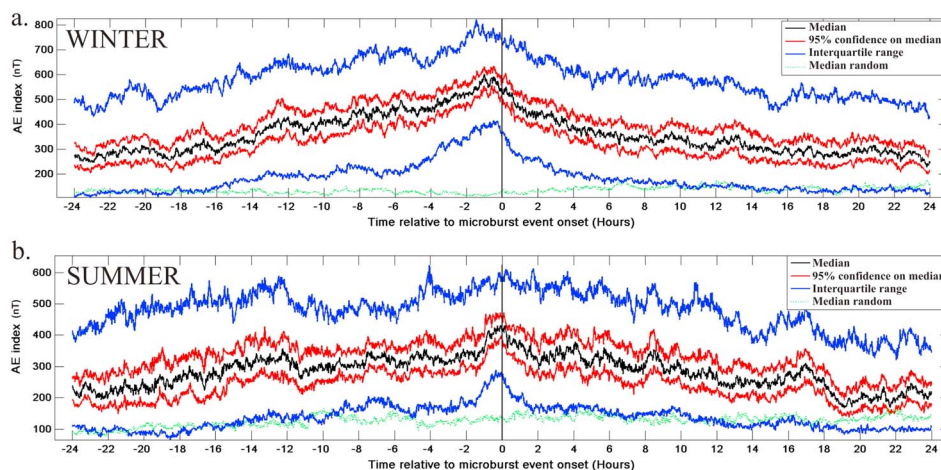


**Figure 6.** As in Figure 5 but for the AE index during the (a) winter time and (b) summer time relativistic microburst events.

periods with significant differences in the medians, namely, 1 h prior to the start of the summer microburst events,  $\sim 3$ –5 h, and  $\sim 10$ –12 h following the summer microburst events.

We have supported this analysis with a manual investigation of the wave amplitude in VELOX. The VELOX quick look plots were visually inspected for wave amplitude increases in the 1–4 kHz frequency range within the  $\pm 1$  h window of the microburst events (following the method outlined in the case studies). We find  $\sim 75\%$  of the winter relativistic microburst events contain VLF wave amplitude increases inside the 2 h window surrounding the microburst event onset. The rounded shape of the VLF wave amplitude increases observed suggests we may be identifying whistler mode chorus waves. Only  $\sim 58\%$  of the random epochs during winter have increased wave amplitude present within the 2 h temporal window encompassing the microburst event onset. A similar trend is found during the summer microburst events, where  $\sim 73\%$  of the microburst events contain VLF wave amplitude increases inside the microburst temporal window. Only  $\sim 50\%$  of the random epochs during summer have increased wave amplitude present within the 2 h temporal window. We suggest the change in chorus-linked wave amplitude enhancements from summer to winter reflects the ionospheric absorption limited detection efficiency of the Halley VELOX.

The final test we conduct to support this analysis is a superposed epoch analysis of the AE index at the time of the relativistic microburst events, presented here as Figure 6 following the layout of Figure 5a. The winter relativistic microbursts are investigated in Figure 6a, and the summer events are investigated in Figure 6b. From Figure 6 it is clear that during both the Halley winter and Halley summer relativistic microbursts events there is an increase in the median AE value when compared to the random events. The increase in the median AE value begins approximately 1.5 days (not shown) prior to the onset of both winter and summer relativistic microburst events and remains elevated for  $\sim 1$  day following both the winter and summer relativistic microburst events. The median AE value reaches a peak  $\sim 30$  min prior to the onset of both summer and winter relativistic microburst events. However, there is a larger increase (increases by 470 nT from the random events) in the median AE value during the winter relativistic microburst events than in the summer relativistic microburst events (increases by 279 nT from the random events). It would appear that, in this study, the summer events are occurring during quieter geomagnetic conditions than the winter events.

The AE index reaches a maximum  $\sim 30$  min prior to the onset of the relativistic microburst events, while the VLF wave amplitude reaches a maximum  $\sim 4$  h after the onset of the microburst events. Therefore, we suggest the change in the wave amplitude seen on the ground might reflect triggering of whistler mode chorus by substorms (Rodger et al., 2016; Smith et al., 1996). However, we have unusually strong substorm activity, producing very large AE values (i.e., median AE of  $\sim 410$ –600 nT). The relativistic microburst events are occurring concurrently with increases in the VLF wave amplitude in the 1–4 kHz frequency range, identified as magnetospheric emissions (either hiss or chorus). On the basis of this analysis we suggest the relativistic microbursts events are in fact occurring concurrently with whistler mode chorus waves (based on the visual inspection).

## 4.2. EMIC Wave Activity

In order to investigate the suggested relationship between EMIC waves and relativistic microbursts, we undertake a superposed epoch analysis of the mean wave power in the 0.1–0.8 Hz frequency range. We also undertake a superposed epoch analysis of the entire spectrogram. Initially, we outline the algorithm used and any data processing and then discuss the results from the superposed epoch analyses. Recall, we use the microburst events occurring from 2005 to 2007.

### 4.2.1. Microburst EMIC Algorithm

Again, we limit our database of relativistic microburst events to those which occur close (within  $\pm 15^\circ$  longitude) to Halley (or Halley's conjugate location) following the method outlined earlier. This reduces our data set of relativistic microburst events to 418 of the 4,471 occurring between 2005 and 2007 ( $\sim 10\%$  of the data set), a combination of 3,773 individual microbursts. We only consider a longitudinal separation following the method of Hendry et al. (2016). We have usable magnetometer data for 295 of the 418 (71%) microburst events.

We have also created a database of random epochs which have been constrained to the same time period (2005–2007) as the true relativistic microburst epochs, and periods of usable magnetometer data. We have 295 random epochs which will give us a baseline comparison with the results of the superposed epoch analysis using the true microburst events.

Furthermore, we have inspected the quick look plots of the Halley magnetometer in order to identify times when the microbursts are associated with clear (strong) EMIC signatures (henceforth referred to as EMIC-linked microburst events) and also times when the microbursts are associated with broadband noise (henceforth referred to as broadband noise linked microburst events). These two data sets will be used as a comparison for all the microburst events. From the inspection we have 75 EMIC-linked microburst events and 127 broadband noise linked microburst events. In addition there were 93 microburst events not linked to either EMIC wave activity or broadband noise.

To test the link between the relativistic microbursts and EMIC waves, we first find the mean wave power measured by the Halley magnetometer in the 0.1–0.8 Hz frequency range at 1 min temporal resolution. We use the lower frequency cutoff of 0.1 Hz to match the EMIC wave definition and the upper frequency cutoff of 0.8 Hz to contain the majority of the EMIC wave activity (based on our visual investigation). We superpose the mean wave power for the 295 relativistic microburst events for which we have usable magnetometer data. Additionally, we investigate the wave power in each frequency band of the 0–1 Hz range through a superposed epoch analysis of the magnetometer spectrogram for the 295 relativistic microburst events. We only consider the  $B_z$  component of the magnetometer as it has lower noise (as seen in the case studies).

### 4.2.2. Superposed Epoch Analysis

Presented here in Figure 7 (following the layout of Figure 5a) is the superposed epoch analysis of the mean wave power in the 0.1–0.8 Hz frequency range, measured by the  $B_z$  component of the magnetometer, at the time of all relativistic microburst events (Figure 7a), EMIC-linked microburst events (Figure 7b), and broadband noise linked microburst events (Figure 7c). From Figure 7a it is clear that during the set of all satellite-observed relativistic microburst events there is an increase in the Halley reported median 0.1–0.8 Hz wave power when compared to the random events. The increase in the median wave power begins approximately 2.5 h prior to the onset of the relativistic microburst events and remains elevated for  $\sim 5$  h following the microburst events. The median wave power peaks at  $\sim 10^{-7}$  nT<sup>2</sup> z, 30 min after the onset of the relativistic microburst epochs. The EMIC (broadband noise)-linked microburst events median wave power peaks at  $\sim 10^{-7}$  nT<sup>2</sup> Hz ( $\sim 10^{-6}$  nT<sup>2</sup> Hz), 30 min after the onset of the relativistic microburst events. The increase in the median wave power begins much earlier and remains elevated longer for the broadband noise-linked events. The EMIC linked events only show increased wave power within a 2 h window of the microburst events, consistent with our identification method. From this analysis we note the wave power increase seen for all microburst events may have an EMIC wave contribution; however, it appears to be dominated by broadband noise.

Figure 8 presents the superposed epoch analysis of the wave power in each frequency band between 0 and 1 Hz for the  $B_z$  component of the magnetometer (hereafter referred to as the superposed spectrogram). Figure 8a is the superposed spectrogram of all of the microburst events over approximately 1 day ( $\pm 8$  h from epoch onset), Figure 8b is the superposed spectrogram of the random epochs, Figure 8c is the EMIC linked microburst events, and Figure 8d is the broadband noise-linked microburst events. The vertical dashed white line in each panel of Figure 8 identifies the onset of the relativistic microburst events.

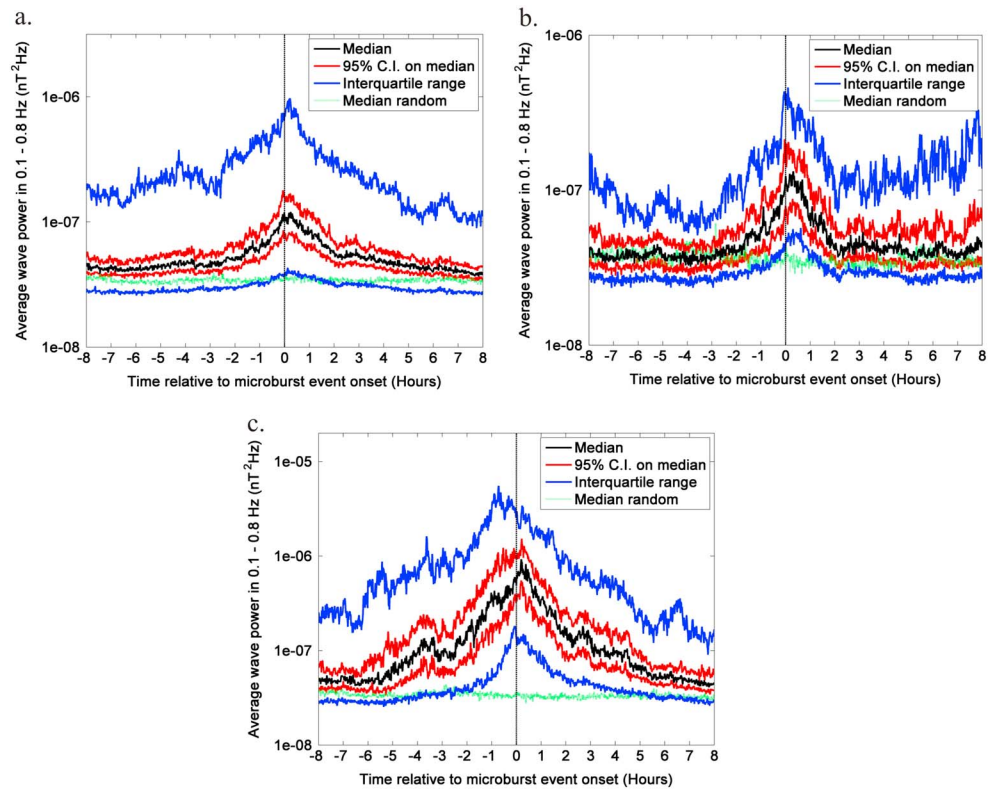


**Figure 7.** As in Figure 5 but for the Bz component of the Halley magnetometer mean wave power in the 0.1–0.8 Hz frequency range at the time of (a) all relativistic microburst events, (b) EMIC linked microburst events, and (c) broadband noise-linked microburst events. Note that C.I. refers to the confidence interval.

From Figure 8a it is clear that during the relativistic microbursts events there is an increase in the median wave power in all frequencies at the time of the relativistic microburst events compared to the random events. The increase in the median wave power begins ~2 h prior to the onset of the relativistic microburst events and remains elevated for ~3 h following the microburst events. The median wave power reaches a peak of  $\sim 10^{-6}$  nT<sup>2</sup> Hz in the 0.1–0.2 Hz frequency range at the onset of the relativistic microburst events. Over the entire 0–1 Hz frequency range we have an average wave power of  $\sim 10^{-7}$  nT<sup>2</sup> Hz, in agreement with Figure 7. However, there is no distinguishable lower limit in the increased wave power of the superposed spectrogram in Figure 8a. When we only consider the EMIC-linked microburst events we note a very subtle lower limit to the wave power at ~0.1 Hz, shown in Figure 8c. Although we have identified clear upper and lower frequency limits for all of the individual EMIC-linked microburst events, the values of these limits were not consistent from event to event. Thus, the average response shown by the superposed epoch method is spread over a range of upper and lower frequency limits. The median wave power for EMIC-linked microburst events peaks in the 0.15–0.4 Hz frequency range at  $\sim 10^{-6}$  nT<sup>2</sup> Hz while for broadband noise-linked microburst events peaks in the 0–0.4 Hz frequency range with much higher wave power (i.e.,  $\sim 10^{-5}$  nT<sup>2</sup> Hz). The superposed spectrogram of all microburst events is more similar to the superposed spectrogram of the broadband noise-linked microburst events than the EMIC-linked microburst events. Therefore, the burst of associated wave power for all microbursts is dominated by broadband noise and not EMIC wave activity. The broadband noise is likely a ULF perturbation generated in the ionosphere by auroral particle precipitation (Arnoldy et al., 1998; Engebretson et al., 2008), likely a result of geomagnetic storms and substorms. As a result of this analysis, we support the earlier suggestion that the increased ULF wave power seen in Figure 7 is not dominated by an increase in EMIC wave activity, but rather dominated by an increase in broadband noise, which is not expected to scatter electrons.

We have supported this analysis with a manual investigation of the wave power in the Bz component of the Halley magnetometer. The magnetometer quick look plots were visually inspected for wave power bursts in the 0–1 Hz frequency range during the 2 h window around the microburst events, following the method

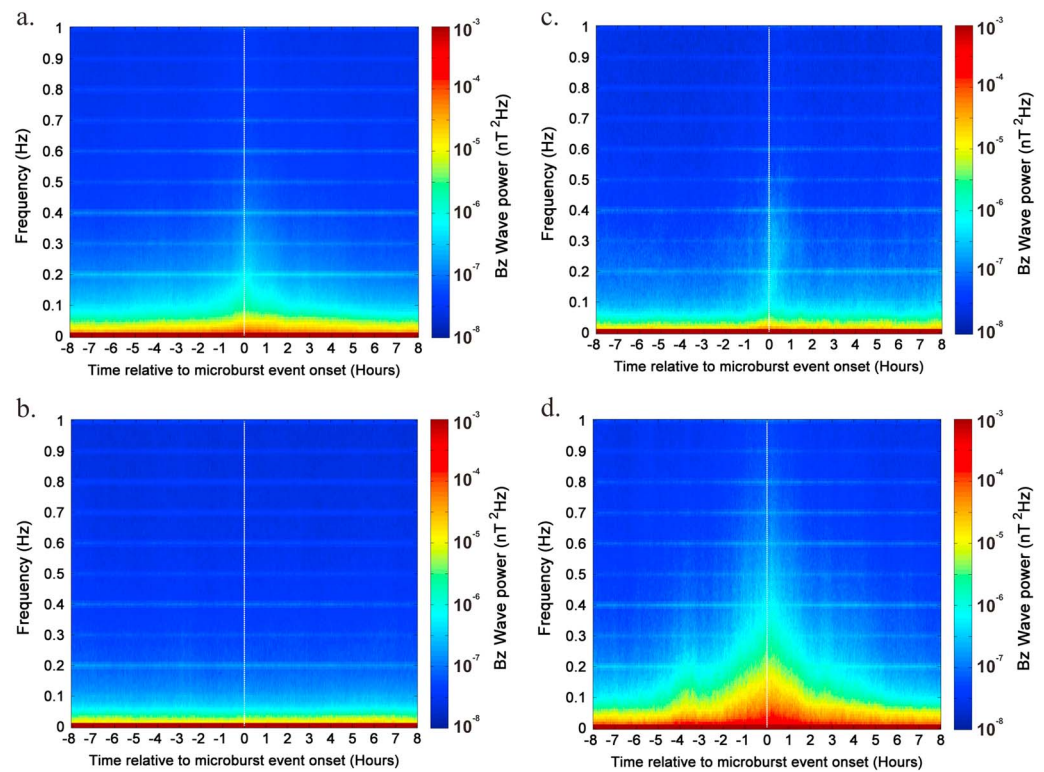


**Figure 8.** A superposed epoch study of the Bz component of the magnetometer wave power present in the 0–1 Hz frequency range at the time of (a) all relativistic microburst events, (b) random epochs, (c) EMIC-linked microburst events, and (d) broadband noise-linked microburst events. The dashed white vertical line denotes the time of the event onset.

outlined in the case studies and Hendry et al. (2016). We find ~25% of the relativistic microburst events contain bursts of wave power in the 0–1 Hz frequency range, which are consistent with EMIC wave activity (i.e., with a clear lower and upper frequency cutoff), within the 2 h temporal window surrounding the microburst event onset. However, we also find ~26% of the random epochs contain bursts of EMIC wave power within the 2 h temporal window encompassing the microburst event onset. This is similar to the random occurrence rate of ~23% found by Hendry et al. (2016). Thus, EMIC wave activity is observed coincident with the relativistic microbursts at the same rate as EMIC waves are coincident with random epochs. This supports the suggestion that the increased wave power seen in the superposed epoch analysis is not a result of increased EMIC activity but is rather due to an increase in broadband noise.

The final test we conduct to support this analysis is a superposed epoch analysis of the AE index at the time of the relativistic microburst events, presented here in Figure 9 (following the layout of Figure 6). Figure 9a shows the median AE values one day either side of the relativistic microburst event onset, while Figure 9b shows the median AE values 3 days either side of the relativistic microburst event onset. From Figure 9 it is clear that during the relativistic microbursts events there is an increase in the median AE value when compared to the random events. The increase in the median AE value begins approximately 1.5 days prior to the onset of the relativistic microburst events and remains elevated for ~1 day following relativistic microburst events. The median AE value reaches a peak of 344.5 nT (baseline value of 95 nT, a difference of 249.5 nT) 1 h prior to the onset of the relativistic microburst events.

Figure 7a demonstrates that there is an increase in wave power in the 0.1–0.8 Hz frequency range at the onset of the relativistic microbursts. Based on this result we might assume the increased wave power was a result of increased EMIC wave activity. However, Figure 8 demonstrates the increased wave power is a result of increased broadband noise (supported by our visual inspection). The increase in the AE index is occurring close (within 2 h) to the onset of the relativistic microbursts, when we also note the largest increase in broadband noise. Therefore, we suggest the increase in broadband noise observed in the Halley magnetometer is a result of magnetic storms or substorms (i.e., reconfiguration), rather than coherent wave activity (Engebretson et al., 2008).

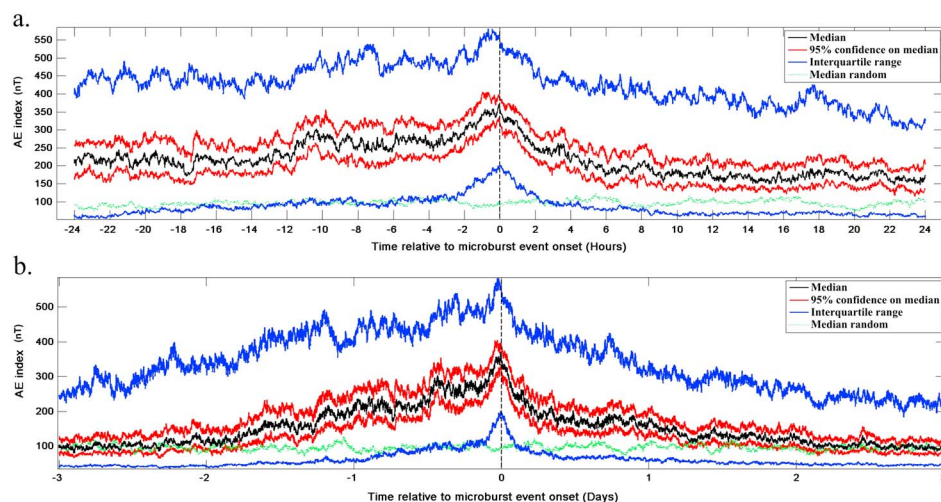


**Figure 9.** As in Figure 6 for the AE index at the time of the relativistic microbursts on (a) hourly timescale and (b) daily timescale.

## 5. Summary and Conclusions

In this paper we presented three case study events of SAMPEX satellite-observed relativistic microburst events occurring concurrently with ground-based wave measurements made at Halley, Antarctica. We have three different wave observations for the three different case studies, relativistic microbursts occurring concurrently with whistler mode chorus waves measured by VELOX, EMIC waves measured by the SCM, and evidence on the ground of both whistler mode chorus and EMIC waves.

Based on the superposed epoch analysis of the Halley VELOX instrument we find there is an increase in VLF wave amplitude in the 1–4 kHz frequency range (the frequency range of whistler mode chorus waves) at the onset of the relativistic microburst events. We suggest the increase in VLF wave amplitude observed in the Halley VELOX instrument is a result of whistler mode chorus wave emissions, consistent with these waves scattering relativistic electrons.

From the superposed epoch analysis of the Halley SCM we find there is an increase in wave power in the 0.1–0.8 Hz frequency range (the frequency range of EMIC waves) at the onset of the relativistic microburst events. However, the increased wave power is typically a result of increased broadband noise and not increased EMIC wave activity. We suggest the increase in broadband noise observed in the Halley magnetometer is a result of magnetic reconfiguration or ULF noise generated in the ionosphere as a result of incoherent energetic particle precipitation, rather than coherent ion cyclotron waves.

Thus, we support the conclusion of Douma et al. (2017) that whistler mode chorus waves are the primary drivers of relativistic microbursts. However, the evidence presented in Case 2 (EMIC wave activity present at the time of the microburst with no whistler mode chorus wave activity observed) does not allow us to rule out EMIC waves as a secondary, and possibly rare, driver of relativistic microbursts.

It should be noted that most of the relativistic microburst events occurred during very high AE values ( $AE > 300$  nT) (Douma et al., 2017). With this level of geomagnetic disturbance it is possible that the plasma waves are not able to propagate through the ionosphere to the ground. This could explain our lack of EMIC wave activity observed on the ground during the microburst events (Engebretson et al., 2008). However, such activity would also be expected to attenuate whistler mode chorus waves.

## References

- Abel, G. A., Freeman, M. P., Smith, A. J., & Reeves, G. D. (2006). Association of substorm chorus events with drift echoes. *Journal of Geophysical Research*, *111*, A11220. <https://doi.org/10.1029/2006JA011860>
- Anderson, R. R., & Maeda, K. (1977). VLF emissions associated with enhanced magnetospheric electrons. *Journal of Geophysical Research*, *82*, 135–146. <https://doi.org/10.1029/JA082i001p00135>
- Anderson, B. R., Shekhar, S., Millan, R. M., Crew, A. B., Spence, H. E., Klumpar, D. M., ... Turner, D. L. (1977). Spatial scale and duration of one microburst region on 13 August 2015. *Journal of Geophysical Research*, *122*, 5949–5964. <https://doi.org/10.1002/2016JA023752>

### Acknowledgments

The authors would like to thank the many individuals involved in the development, operation, and maintenance of SAMPEX, the Halley search coil magnetometer, and the Halley VELOX instrument. Support for the Halley search coil magnetometer was provided by U.S. National Science Foundation grants PLR-1341493 to Augsburg College and PLR-1341677 to the University of New Hampshire. E. D. was supported by the University of Otago via a Fanny Evans PhD scholarship for women. Data availability is described at the following websites: <http://www.srl.caltech.edu/sampex/DataCenter/index.html> (SAMPEX), <http://psddb.nerc-bas.ac.uk/data/access/coverage.php?class=101&menu=1&old=7&source=1&script=1> (Halley magnetometer), [wcd.kugi.kyoto-u.ac.jp](http://wcd.kugi.kyoto-u.ac.jp) (AE), and <http://psddb.nerc-bas.ac.uk/data/access/coverage.php?menu=1,7&source=1&script=1&class=140> (Halley VELOX).

- Arnoldy, R. L., Cahill, Jr., Engebretson, M. J., Lanzerotti, L. J., & Wolfe, A. (1998). Review of hydromagnetic wave studies in the Antarctic. *Reviews of Geophysics*, *26*, 181–207. <https://doi.org/10.1029/RG026i001p00181>
- Baker, D. N., Mason, G. M., Figueroa, O., Colon, G., Watzin, J. G., & Aleman, R. M. (1993). An overview of the Solar, Anomalous, and Magnetospheric Particle Explorer (SAMPEX) mission. *IEEE Transactions on Geoscience and Remote Sensing*, *31*, 531–541. <https://doi.org/10.1109/36.225519>
- Blake, J. B., Looper, M. D., Baker, D. N., Nakamura, R., Klecker, B., & Hovestadt, D. (1996). New high temporal and spatial resolution measurements by SAMPEX of the precipitation of relativistic electrons. *Advances in Space Research*, *18*, 171–186. [https://doi.org/10.1016/0273-1177\(95\)00969-8](https://doi.org/10.1016/0273-1177(95)00969-8)
- Blum, L., Li, X., & Denton, M. (2015). Rapid MeV electron precipitation as observed by SAMPEX/HILT during high-speed stream-driven storms. *Journal of Geophysical Research: Space Physics*, *120*, 3783–3794. <https://doi.org/10.1002/2014JA020633>
- Boscher, D., Bourdarie, S., O'Brien, P., & Guild, T. (2015). IRBEM-lib—Project home page. Retrieved from <http://irbem.sourceforge.net/>
- Breneman, A. W., Crew, A., Sample, J., Klumpar, D., Johnson, A., Agapitov, O., ... Kletzing, C. A. (2017). Observations directly linking relativistic electron microbursts to whistler mode chorus: Van Allen Probes and FIREBIRD II. *Geophysical Research Letters*, *44*, 11,265–11,272. <https://doi.org/10.1002/2017GL075001>
- Cliilverd, M. A., Rodger, C. J., & Ulich, T. (2006). The importance of atmospheric precipitation in storm-time relativistic electron flux drop outs. *Geophysical Research Letters*, *33*, L01102. <https://doi.org/10.1029/2005GL024661>
- Collier, A., & Hughes, A. (2004). Modelling substorm chorus events in terms of dispersive azimuthal drift. *Annales Geophysicae*, *22*, 4311–4327. <https://doi.org/10.5194/angeo-22-4311-2004>
- Crew, A. B., Spence, H. E., Blake, J. B., Klumpar, D. M., Larsen, B. A., O'Brien, T. P., ... Widholm, M. (2016). First multipoint in situ observations of electron microbursts: Initial results from the NSF FIREBIRD II mission. *Journal of Geophysical Research: Space Physics*, *121*, 5272–5283. <https://doi.org/10.1002/2016JA022485>
- Dietrich, S., Rodger, C. J., Cliilverd, M. A., Bortnik, J., & Raita, T. (2010). Relativistic microburst storm characteristics: Combined satellite and ground-based observations. *Journal of Geophysical Research*, *115*, A12240. <https://doi.org/10.1029/2010JA015777>
- Douma, E., Rodger, C. J., Blum, L. W., & Cliilverd, M. A. (2017). Occurrence characteristics of relativistic electron microbursts from SAMPEX observations. *Journal of Geophysical Research: Space Physics*, *122*, 8096–8107. <https://doi.org/10.1002/2017JA024067>
- Engebretson, M. J., Lessard, M. R., Bortnik, J., Green, J. C., Horne, R. B., Detrick, D. L., ... Rose, M. C. (2008). Pc1–Pc2 waves and energetic particle precipitation during and after magnetic storms: Superposed epoch analysis and case studies. *Journal of Geophysical Research*, *113*, A01211. <https://doi.org/10.1029/2007JA012362>
- Fennell, J. F., Roeder, J. L., Kurth, W. S., Henderson, M. G., Larsen, B. A., Hospodarsky, G., ... Reeves, G. D. (2014). Van Allen Probes observations of direct wave-particle interactions. *Geophysical Research Letters*, *41*, 1869–1875. <https://doi.org/10.1002/2013GL059165>
- Hendry, A. T., Rodger, C. J., Cliilverd, M. A., Engebretson, M. J., Mann, I. R., Lessard, M. R., ... Milling, D. K. (2016). Confirmation of EMIC wave-driven relativistic electron precipitation. *Journal of Geophysical Research: Space Physics*, *121*, 5366–5383. <https://doi.org/10.1002/2015JA022224>
- Johnston, W. R., & Anderson, P. C. (2010). Storm time occurrence of relativistic electron microbursts in relation to the plasmopause. *Journal of Geophysical Research*, *115*, A02205. <https://doi.org/10.1029/2009JA014328>
- Jordanova, V. K., Albert, J., & Miyoshi, Y. (2008). Relativistic electron precipitation by EMIC waves from self-consistent global simulations. *Journal of Geophysical Research*, *113*, A00A10. <https://doi.org/10.1029/2008JA013239>
- Kersten, K., Cattell, C. A., Breneman, A., Goetz, K., Kellogg, P. J., Wygant, J. R., ... Roth, I. (2011). Observation of relativistic electron microbursts in conjunction with intense radiation belt whistler-mode waves. *Geophysical Research Letters*, *38*, L08107. <https://doi.org/10.1029/2011GL046810>
- Klecker, B., Hovestadt, D., Scholer, M., Arbing, H., Ertl, M., Kastle, H., ... Mabry, D. (1993). HILT: A heavy ion large area proportional counter telescope for solar and anomalous cosmic rays. *IEEE Transactions of Geoscience and Remote Sensing*, *31*, 542–548. <https://doi.org/10.1109/36.225520>
- Kubota, Y., & Omura, Y. (2017). Rapid precipitation of radiation belt electrons induced by EMIC rising tone emissions localized in longitude inside and outside the plasmopause. *Journal of Geophysical Research: Space Physics*, *122*, 293–309. <https://doi.org/10.1002/2016JA023267>
- Kurita, S., Miyoshi, Y., Blake, J. B., Reeves, G. D., & Kletzing, C. A. (2016). Relativistic electron microbursts and variations in trapped MeV electron fluxes during the 8–9 October 2012 storm: SAMPEX and Van Allen Probes observations. *Geophysical Research Letters*, *43*, 3017–3025. <https://doi.org/10.1002/2016GL068260>
- LeDocq, M. J., Gurnett, D. A., & Hospodarsky, G. B. (1998). Chorus source locations from VLF poynnting flux measurements with the Polar spacecraft. *Geophysical Research Letters*, *25*, 4063–4066. <https://doi.org/10.1029/1998GL900071>
- Li, W., Thorne, R. M., Angelopoulos, V., Bortnik, J., Cully, C. M., Ni, B., ... Magnes, W. (2009). Global distribution of whistler-mode chorus waves observed on the THEMIS spacecraft. *Geophysical Research Letters*, *36*, L09104. <https://doi.org/10.1029/2009GL037595>
- Lorentzen, K. R., Looper, M. D., & Blake, J. B. (2001). Relativistic electron microbursts during the GEM storms. *Geophysical Research Letters*, *28*, 2573–2576. <https://doi.org/10.1029/2001GL012926>
- Lorentzen, K. R., Blake, J. B., Inan, U. S., & Bortnik, J. (2001). Observations of relativistic electron microbursts in association with VLF chorus. *Journal of Geophysical Research*, *106*, 6017–6027. <https://doi.org/10.1029/2000JA003018>
- Loto'aniu, T. M., Fraser, B. J., & Waters, C. L. (2005). Propagation of electromagnetic ion cyclotron wave energy in the magnetosphere. *Journal of Geophysical Research*, *110*, A07214. <https://doi.org/10.1029/2004JA010816>
- Meredith, N. P., Horne, R. B., Kersten, T., Fraser, B. J., & Grew, R. S. (2014). Global morphology and spectral properties of EMIC waves derived from CRRES observations. *Journal of Geophysical Research: Space Physics*, *119*, 5328–5342. <https://doi.org/10.1002/2014JA020064>
- Miyoshi, Y., Oyama, S., Saito, S., Fujiwara, H., Kataoka, R., Ebihara, Y., ... Tsuchiya, F. (2015). Energetic electron precipitation associated with pulsating aurora: EISCAT and Van Allen Probes observations. *Journal of Geophysical Research: Space Physics*, *120*, 2754–2766. <https://doi.org/10.1002/2014JA020690>
- Nakamura, R., Isowa, M., Kamide, Y., Baker, D. N., Blake, J. B., & Looper, M. (2000). SAMPEX observations of precipitation bursts in the outer radiation belt. *Journal of Geophysical Research*, *105*, 15,875–15,885. <https://doi.org/10.1029/2000JA900018>
- O'Brien, T. P., Lorentzen, K. R., Mann, I. R., Meredith, N. P., Blake, J. B., Fennell, J. F., ... Anderson, R. R. (2003). Energization of relativistic electrons in the presence of ULF wave power and MeV microbursts: Evidence for dual ULF and VLF acceleration. *Journal of Geophysical Research*, *108*, SMP11. <https://doi.org/10.1029/2002JA009784>
- Omura, Y., & Zhao, Q. (2013). Relativistic electron microbursts due to nonlinear pitch angle scattering by EMIC triggered emissions. *Journal of Geophysical Research: Space Physics*, *118*, 5008–5020. <https://doi.org/10.1002/jgra.50477>
- Reeves, G. D., McAdams, K. L., Friedel, R. H. W., & O'Brien, T. P. (2003). Acceleration and loss of relativistic electrons during geomagnetic storms. *Geophysical Research Letters*, *30*(10), 1529. <https://doi.org/10.1029/2002GL016513>

- Rodger, C. J., Clilverd, M. A., Nunn, D., Verronen, P. T., Bortnik, J., & Turunen, E. (2007). Storm time, short-lived bursts of relativistic electron precipitation detected by subionospheric radio wave propagation. *Journal of Geophysical Research*, *112*, A07301. <https://doi.org/10.1029/2007JA012347>
- Rodger, C. J., Cresswell-Moorcock, K., & Clilverd, M. A. (2016). Nature's Grand Experiment: Linkage between magnetospheric convection and the radiation belts. *Journal of Geophysical Research: Space Physics*, *121*, 171–189. <https://doi.org/10.1002/2015JA021537>
- Saikin, A. A., Zhang, J.-C., Allen, R. C., Smith, C. W., Kistler, L. M., Spence, H. E., ... Jordanova, V. K. (2015). The occurrence and wave properties of H<sup>+</sup>-, He<sup>+</sup>-, and O<sup>+</sup>-band EMIC waves observed by the Van Allen Probes. *Journal of Geophysical Research: Space Physics*, *120*, 7477–7492. <https://doi.org/10.1002/2016JA022523>
- Saito, S., Miyoshi, Y., & Seki, K. (2012). Relativistic electron microbursts associated with whistler chorus rising tone elements: GEMSIS-RBW simulations. *Journal of Geophysical Research*, *117*, A10206. <https://doi.org/10.1029/2012JA018020>
- Santolik, O., Gurnett, D. A., Pickett, J. S., Parrot, M., & Cornilleau-Wehrin, N. (2003). Spatio-temporal structure of storm-time chorus. *Journal of Geophysical Research Space Physics*, *108*(A7), 1278. <https://doi.org/10.1029/2002JA009791>
- Seppälä, A., Clilverd, M. A., Rodger, C. J., Verronen, P. T., & Turunen, E. (2008). The effects of hard-spectra solar proton events on the middle atmosphere. *Journal of Geophysical Research*, *113*, A11311. <https://doi.org/10.1029/2008JA013517>
- Smith, A. J. (1995). VELOX: A new VLF/ELF receiver in Antarctica for the Global Geospace Science mission. *Journal of Atmospheric and Terrestrial Physics*, *57*, 507–524. [https://doi.org/10.1016/0021-9169\(94\)00078-3](https://doi.org/10.1016/0021-9169(94)00078-3)
- Smith, A. J., Freeman, M. P., & Reeves, G. D. (1996). Post midnight VLF chorus events, a substorm signature observed at the ground near L = 4. *Journal of Geophysical Research*, *101*, 24,641–24,653. <https://doi.org/10.1029/96JA02236>
- Smith, A. J., Freeman, M. P., Wickett, M. G., & Cox, B. D. (1999). On the relationship between the magnetic and VLF signatures of the substorm expansion phase. *Journal of Geophysical Physics*, *104*, 12,351–12,360. <https://doi.org/10.1029/1998JA900184>
- Smith, A. J., Meredith, N. P., & O'Brien, T. P. (2004). Differences in ground-observed chorus in geomagnetic storms with and without enhanced relativistic electron fluxes. *Journal of Geophysical Research*, *109*, A11204. <https://doi.org/10.1029/2004JA010491>
- Smith, A. J., Horne, R. B., & Meredith, N. P. (2010). The statistics of natural ELF/VLF waves derived from a long continuous set of ground-based observations at high latitude. *Journal of Atmospheric and Solar-Terrestrial Physics*, *72*, 463–475. <https://doi.org/10.1016/j.jastp.2009.12.018>
- Thorne, R. M., O'Brien, T. P., Shprits, Y. Y., Summers, D., & Horne, R. B. (2005). Timescale for MeV electron microburst loss during geomagnetic storms. *Journal of Geophysical Research*, *110*, A09202. <https://doi.org/10.1029/2004JA010882>
- Troitskaya, V. A. (1961). Pulsation of the Earth's electromagnetic field with periods of 1 to 15 seconds and their connection with phenomena in the high atmosphere. *Journal of Geophysical Research*, *66*, 5–18. <https://doi.org/10.1029/JZ066i001p00005>
- Tsurutani, B. T., & Smith, E. J. (1974). Postmidnight chorus: A substorm phenomenon. *Journal of Geophysical Research*, *79*, 118–127. <https://doi.org/10.1029/JA079i001p00118>
- Tsyganenko, N. A. (1989). A magnetospheric magnetic field model with a warped tail current sheet. *Planetary and Space Science*, *37*, 5–20. [https://doi.org/10.1016/0032-0633\(89\)90066-4](https://doi.org/10.1016/0032-0633(89)90066-4)
- Usanova, M. E., Mann, I. R., Bortnik, J., Shao, L., & Angelopoulos, V. (2012). THEMIS observations of electromagnetic ion cyclotron wave occurrence: Dependence on AE, SYMH, and solar wind dynamic pressure. *Journal of Geophysical Research*, *117*, A10218. <https://doi.org/10.1029/2012JA018049>